Improved bearing and range estimation via high-order subspace based Unitary ESPRIT

Martin Haardt
Inst. of Network Theory & Circuit Design
Technical University of Munich
D-80290 Munich, Germany

Raghu N. Challa
Qualcomm Incorporated
Morehouse Rd., T-560H
San Diego, CA 92122, USA

Sanyogita Shamsunder
Department of Electrical Engineering
Colorado State University
Fort Collins, CO 80523, USA

Abstract

Two new algorithms for the passive localization of near-field sources with a uniform linear array (ULA) are presented and compared in this paper. They exploit multiple invariances among certain fourth-order cross-cumulant matrices of non-zero and zero lags, respectively. Both algorithms utilize 2-D Unitary ESPRIT to obtain automatically paired bearing and range estimates. The resulting closed-form subspace-based methods incorporate forward-backward averaging, use efficient real-valued processing of the cumulant data, and outperform previously proposed high-order subspace-based algorithms for the localization of near-field sources. In the limit, the presented schemes also work for far-field sources.

1. Introduction

Direction of arrival (DOA) estimation is an important problem in sensor array signal processing. The information about the source locations, for example, can be used for source separation and enhancement of signal to noise ratios. In the past, many algorithms addressed the estimation of azimuth and/or elevation of far-field sources which are known to introduce linear phase shifts in signals collected by the sensors owing to the linear curvature of the plane wave-fronts. As the sources move into the *Fresnel* region of the array, the range information needs to be incorporated into the signal model for accurate source separation. Usually the polynomial phase introduced by the spherical wavefronts of a near-field source can be well approximated by a second order polynomial.

Consider a uniform linear array (ULA) of M identical, omnidirectional sensors with inter-element spacing Δ and sensor indices $k \in \mathcal{K}$, where the set of sensor indices is given by

$$\mathcal{K} = \{k_{\min}, \ldots, k_{\max}\} = \begin{cases} \{-\frac{M-2}{2}, \ldots, -1, 0, 1, \ldots, \frac{M}{2}\} & \text{if } M \text{ is even} \\ \{-\frac{M-1}{2}, \ldots, -1, 0, 1, \ldots, \frac{M-1}{2}\} & \text{if } M \text{ is odd.} \end{cases}$$

Assume that the ULA is in the near-field of d narrowband, co-channel sources with wavelength λ. Each source is located at an angle θ_i and at range r_i, $1 \leq i \leq d$, both measured with respect to the reference sensor with index 0. Then, the noise-corrupted array measurements at the kth sensor can be approximated as

$$x_k(t) = \sum_{i=1}^{d} s_i(t) e^{j(\mu_i k + \zeta_i k^2)} + n_k(t), \qquad (1)$$

for $k \in \mathcal{K}$, where $\{n_k(t)\}$ denotes (circular) white Gaussian noise. The signal phase has two components: (i) $\mu_i = -2\pi \frac{\Delta}{\lambda} \sin\theta_i$ corresponds to the far-field phase and is dependent only on azimuth, (ii) $\zeta_i = \pi \frac{\Delta^2}{\lambda r_i} \cos^2\theta_i$ is the extra term included to approximate the effect of spherical curvature of the wavefronts and is a function of both azimuth and range. Thus to localize a near-field source, one needs to estimate both μ_i and ζ_i.

Due to the non-linear nature of the signal phase, the previous approaches based on second-order statistics require an expensive 2-D search and suffer from poor resolution and pairing problems [3, 4, 5]. Recent high-resolution approaches to the near-field problem [1] exploited the invariant properties of cumulant matrices. In [1], it was shown that nonlinear cumulant processing can map the ULA in the near-field scenario to three

1058-6393/97 $10.00 © 1997 IEEE

ULAs in a virtual far-field scenario. The invariant subspaces generated by these arrays were exploited, and a TLS-ESPRIT like algorithm was proposed for generating paired estimates of $\{azimuth,\ range\}$ for multiple sources.

In this paper, we take an alternative view point and propose solutions which exploit the centro-symmetry of fourth-order cross-cumulant matrices. The new algorithms are based on the idea that as a result of the nonlinear operations involved in cumulant computation, the observations from a 1-D linear array in the presence of near-field sources can be transformed into pseudo-data collected from a virtual rectangular array observing virtual far-field sources. The azimuth and elevation of these virtual far-field sources will be functions of $\{\mu_i, \zeta_i\}$ in the original data.

For the signal in (1), the fourth-order cross-cumulant of the set of sensors $(-k+p)$, $(k-p)$, $(\ell-q)$, and $(\ell-q+1)$ is

$$\begin{aligned} & c_{p,q}(\tau, k, \ell) \\ & \triangleq \ \mathrm{cum}\{x^H_{-k+p}(t+\tau), x_{k-p}(t), x^H_{\ell-q}(t), x_{\ell-q+1}(t)\} \\ & = \ \sum_{i=1}^{d} c_{s_i}(\tau) e^{\mathrm{j}[2\mu_i k + 2\zeta_i \ell + (1-2p)\mu_i + (1-2q)\zeta_i]}, \qquad (2) \end{aligned}$$

where $c_{s_i}(\tau) \triangleq \mathrm{cum}\{s_i^H(t+\tau), s_i(t), s_i^H(t), s_i(t)\}$ denotes the fourth-order cumulant of the source signal $s_i(t)$.

Thus the fourth-order cross-cumulant in (2) effectively linearizes the non-linear phase of (1) and resembles a single snapshot by a sensor recording the data from an equivalent far-field source. The linear variation of the cumulant phase with the sensor indices and their dependence on lags τ are exploited in the sequel, to generate "pseudo data" collected from a "pseudo rectangular array" observing virtual far-field sources to which existing far-field techniques can be applied for source parameter estimation. The two algorithms discussed, differ in the manner in which the virtual array data is generated and suggest a tradeoff between the array size and memory of the source signals. The first of the two algorithms can be applied to bigger arrays and when the sources are known to have short memory, while the second algorithm is useful in localizing source signals with non-vanishing higher cumulant lags.

The two algorithms presented are based on 2-D Unitary ESPRIT [7, 8] and exploit equation (2). Unitary ESPRIT is an ESPRIT-type high-resolution frequency estimation technique that constrains the estimated phase factors to the unit circle and is formulated in terms of real-valued computations throughout [12]. Recently, Unitary ESPRIT has been extended to the two-dimensional case to estimate automatically paired (spatial) frequency pairs via a new closed-form procedure, neither requiring any search nor any other heuristic pairing strategy [7, 8]. 3-D localization algorithms using cumulant Unitary ESPRIT can be found [2].

2. Zero Lag Cumulants

In the first case, only the source cumulants $c_{s_i}(\tau)$ of lag $\tau = 0$ have to be non-vanishing. The cross-cumulants $c_{p,q}(0, k, \ell)$ can be collected for $(k_{\min} + k_0) \leq k, \ell \leq (k_{\max} - 2)$ in a matrix $\mathcal{C}(p,q)$ of size $(M - k_0 - 2) \times (M - k_0 - 2)$ as defined in (3) on the top of the next page. From (2), $\mathcal{C}(p,q)$ can be expressed as

$$\mathcal{C}(p,q) = \sum_{i=1}^{d} \boldsymbol{a}(\mu_i)\boldsymbol{a}^T(\zeta_i) c_{s_i} e^{\mathrm{j}[(1-2p)\mu_i + (1-2q)\zeta_i]}, \quad (4)$$

where $\boldsymbol{a}(\mu_i)$ and $\boldsymbol{a}(\zeta_i)$ are Vandermonde vectors given by

$$\begin{aligned} \boldsymbol{a}(\mu_i) &= \left[\ e^{\mathrm{j}2(k_{\min}+k_0)\mu_i} \ \cdots \ 1 \ \cdots \ e^{\mathrm{j}2(k_{\max}-2)\mu_i}\ \right]^{\mathrm{T}} \\ \boldsymbol{a}(\zeta_i) &= \left[\ e^{\mathrm{j}2(k_{\min}+k_0)\zeta_i} \ \cdots \ 1 \ \cdots \ e^{\mathrm{j}2(k_{\max}-2)\zeta_i}\ \right]^{\mathrm{T}}. \end{aligned}$$

Clearly, the arrangement in (4) resembles the measurement matrix of an omnidirectional URA observing d far-field sources, with $M_{\mathrm{v}} = (M - k_0 - 2) \times (M - k_0 - 2)$ virtual sensor elements. This concept of transforming the near-field scenario to a far-field scenario is depicted in Figure 1. For the sake of mathematical convenience,

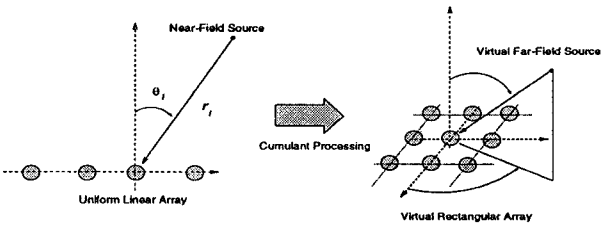

Figure 1: Transformation from near-field scenario to virtual far-field scenario.

each snapshot from the URA is stacked as a column vector by applying vec$\{\cdot\}$-operator to $\mathcal{C}(p,q)$ to yield

$$\begin{aligned} c(p,q) &= \mathrm{vec}\{\mathcal{C}(p,q)\} \qquad (5) \\ &= \sum_{i=1}^{d} \boldsymbol{a}(\mu_i, \zeta_i) c_{s_i} e^{\mathrm{j}[(1-2p)\mu_i + (1-2q)\zeta_i]}, \end{aligned}$$

where the vectors $\boldsymbol{a}(\mu_i, \zeta_i) = \boldsymbol{a}(\zeta_i) \otimes \boldsymbol{a}(\mu_i)$ can be interpreted as the steering vectors of the virtual URA. By varying the indices p and q from -1 to k_0, $N_{\mathrm{v}} =$

$$\mathcal{C}(p,q) = \begin{bmatrix} c_{p,q}(0,k_{\min}+k_0,k_{\min}+k_0) & c_{p,q}(0,k_{\min}+k_0,k_{\min}+k_0+1) & \cdots & c_{p,q}(0,k_{\min}+k_0,k_{\max}-2) \\ c_{p,q}(0,k_{\min}+k_0+1,k_{\min}+k_0) & c_{p,q}(0,k_{\min}+k_0+1,k_{\min}+k_0+1) & \cdots & c_{p,q}(0,k_{\min}+k_0+1,k_{\max}-2) \\ \vdots & \vdots & \ddots & \vdots \\ c_{p,q}(0,k_{\max}-2,k_{\min}+k_0) & c_{p,q}(0,k_{\max}-2,k_{\min}+k_0+1) & \cdots & c_{p,q}(0,k_{\max}-2,k_{\max}-2) \end{bmatrix}. \quad (3)$$

$(2+k_0)^2$ virtual snapshots are generated from (5) and collected in a matrix as

$$\boldsymbol{C} = \begin{bmatrix} \boldsymbol{c}(-1,-1) & \boldsymbol{c}(0,-1) & \cdots & \boldsymbol{c}(k_0,k_0) \end{bmatrix}, \quad (6)$$

which is of size $M_{\mathrm{v}} \times N_{\mathrm{v}}$, and can be thought of as a cumulant domain data matrix.

2.1. Dual Invariance Structure

Let the virtual 2-D array steering matrix be defined as

$$\boldsymbol{A}_{\mathrm{v}} = \begin{bmatrix} \boldsymbol{a}(\mu_1,\zeta_1) & \boldsymbol{a}(\mu_2,\zeta_2) & \cdots & \boldsymbol{a}(\mu_d,\zeta_d) \end{bmatrix}.$$

Then the two pairs of selection matrices

$$\begin{aligned} \boldsymbol{J}_{\mu 1} &= \boldsymbol{I}_{M-k_0-2} \otimes \boldsymbol{J}_1^{(M-k_0-2)} \\ \boldsymbol{J}_{\mu 2} &= \boldsymbol{I}_{M-k_0-2} \otimes \boldsymbol{J}_2^{(M-k_0-2)} \\ \boldsymbol{J}_{\zeta 1} &= \boldsymbol{J}_1^{(M-k_0-2)} \otimes \boldsymbol{I}_{M-k_0-2} \\ \boldsymbol{J}_{\zeta 2} &= \boldsymbol{J}_2^{(M-k_0-2)} \otimes \boldsymbol{I}_{M-k_0-2}, \end{aligned}$$

where $\boldsymbol{J}_1^{(M-k_0-2)} = \begin{bmatrix} \boldsymbol{I}_{M-k_0-3} & \mathrm{o} \end{bmatrix}$ and $\boldsymbol{J}_2^{(M-k_0-2)} = \begin{bmatrix} \mathrm{o} & \boldsymbol{I}_{M-k_0-3} \end{bmatrix}$

are of size $(M-k_0-3)\times(M-k_0-2)$, cause the virtual 2-D array steering matrix to satisfy the following two invariance properties,

$$\boldsymbol{J}_{\mu 1}\boldsymbol{A}_{\mathrm{v}}\boldsymbol{\Phi}_{\mu} = \boldsymbol{J}_{\mu 2}\boldsymbol{A}_{\mathrm{v}} \quad \text{and} \quad \boldsymbol{J}_{\zeta 1}\boldsymbol{A}_{\mathrm{v}}\boldsymbol{\Phi}_{\zeta} = \boldsymbol{J}_{\zeta 2}\boldsymbol{A}_{\mathrm{v}}. \quad (7)$$

Here, the diagonal matrices

$$\boldsymbol{\Phi}_{\mu} = \mathrm{diag}\left\{e^{\mathrm{j}2\mu_i}\right\}_{i=1}^{d} \quad \text{and} \quad \boldsymbol{\Phi}_{\zeta} = \mathrm{diag}\left\{e^{\mathrm{j}2\zeta_i}\right\}_{i=1}^{d}$$

are unitary and contain the desired information about the DOA and range parameters. To avoid ambiguities in the estimation of the DOAs θ_i $(-90^\circ < \theta_i < 90^\circ)$, the inter-element spacing Δ should be restricted to $\Delta \le \lambda/4$. Notice that the two invariance equations (7) are of size $m_{\mathrm{v}} \times d$, where $m_{\mathrm{v}} = (M-k_0-3)\cdot(M-k_0-2)$.

3. 2-D Unitary ESPRIT

2-D Unitary ESPRIT in element space or DFT beamspace can directly be applied to the near-field localization problem by replacing the data matrix $\boldsymbol{X}$ of the element space or DFT beamspace version of 2-D Unitary ESPRIT [7, 8] by the sample estimated cross-cumulant matrix $\widehat{\boldsymbol{C}}$. In this section, we briefly summarize the element space version, while the DFT beamspace implementation of 2-D Unitary ESPRIT for near-field source localization follows along the same lines. Let us define left $\boldsymbol{\Pi}$-real matrices [11, 12] as matrices $\boldsymbol{Q} \in \mathbb{C}^{M\times M}$ satisfying $\boldsymbol{\Pi}_M\overline{\boldsymbol{Q}} = \boldsymbol{Q}$, where the overbar denotes complex conjugation without transposition. For any positive integer M, $\boldsymbol{I}_M$ denotes the identity matrix of size $M \times M$ and $\boldsymbol{\Pi}_M$ the $M \times M$ exchange matrix with ones on its antidiagonal and zeros elsewhere. The unitary matrix

$$\boldsymbol{Q}_{2q+1} = \frac{1}{\sqrt{2}} \begin{bmatrix} \boldsymbol{I}_q & \mathrm{o} & \mathrm{j}\,\boldsymbol{I}_q \\ \mathrm{o}^T & \sqrt{2} & \mathrm{o}^T \\ \boldsymbol{\Pi}_q & \mathrm{o} & -\mathrm{j}\,\boldsymbol{\Pi}_q \end{bmatrix}, \quad (8)$$

for example, is left $\boldsymbol{\Pi}$-real of odd order. A unitary left $\boldsymbol{\Pi}$-real matrix of size $2q \times 2q$ is obtained from (8) by dropping its center row and center column. More left $\boldsymbol{\Pi}$-real matrices can be constructed by post-multiplying a left $\boldsymbol{\Pi}$-real matrix $\boldsymbol{Q}$ by an arbitrary real matrix $\boldsymbol{R}$, i.e., every matrix $\boldsymbol{Q}\,\boldsymbol{R}$ is left $\boldsymbol{\Pi}$-real.

In the first step of Unitary ESPRIT [7, 8], forward-backward averaging is achieved by transforming the estimated cross-cumulant matrix $\widehat{\boldsymbol{C}}$ into the real-valued matrix[1]

$$\mathcal{T}(\widehat{\boldsymbol{C}}) = \boldsymbol{Q}_{M_{\mathrm{v}}}^H \begin{bmatrix} \widehat{\boldsymbol{C}} & \boldsymbol{\Pi}_{M_{\mathrm{v}}}\overline{\widehat{\boldsymbol{C}}}\,\boldsymbol{\Pi}_{N_{\mathrm{v}}} \end{bmatrix} \boldsymbol{Q}_{2N_{\mathrm{v}}} \in \mathbb{R}^{M_{\mathrm{v}}\times 2N_{\mathrm{v}}}.$$

Its d dominant left singular vectors $\boldsymbol{E}_s \in \mathbb{R}^{M_{\mathrm{v}}\times d}$ are determined through a real-valued SVD of $\mathcal{T}(\widehat{\boldsymbol{C}})$

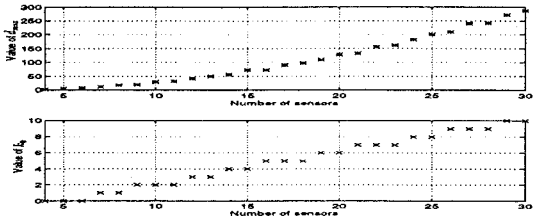

Figure 2: Recommended values of k_0 and the resulting values of $d_{\max}$ as a function of the number of sensors M of the ULA.

[1] If the the left Π-real matrices Q_M and Q_{2N} are chosen according to (8) and M is even, an efficient computation of the transformation $\mathcal{T}(\widehat{C}) \in \mathbb{R}^{M\times 2N}$ from the complex-valued data matrix X only requires $M_{\mathrm{v}} \cdot 2N_{\mathrm{v}}$ real additions and no multiplication [12].

(square-root approach). Alternatively, they can be computed through a real-valued eigendecomposition of $\mathcal{T}(\widehat{C})\mathcal{T}^H(\widehat{C})$ (covariance approach). Based on the two invariance properties of $\boldsymbol{A}_{\mathrm{v}}$ in (7), the following two real-valued invariance equations are formed

$$\begin{aligned} \boldsymbol{K}_{\mu 1}\boldsymbol{E}_s\boldsymbol{\Upsilon}_\mu &\approx \boldsymbol{K}_{\mu 2}\boldsymbol{E}_s \in \mathbb{R}^{m_{\mathrm{v}}\times d} \quad \text{and} \\ \boldsymbol{K}_{\zeta 1}\boldsymbol{E}_s\boldsymbol{\Upsilon}_\zeta &\approx \boldsymbol{K}_{\zeta 2}\boldsymbol{E}_s \in \mathbb{R}^{m_{\mathrm{v}}\times d}, \end{aligned} \tag{9}$$

where the four transformed selection matrices are constructed from the selection matrices $\boldsymbol{J}_{\mu 2}$ and $\boldsymbol{J}_{\zeta 2}$ as

$$\begin{aligned} \boldsymbol{K}_{\mu 1} &= 2\cdot\mathrm{Re}\{\boldsymbol{Q}_{m_{\mathrm{v}}}^H\boldsymbol{J}_{\mu 2}\boldsymbol{Q}_{M_{\mathrm{v}}}\} \\ \boldsymbol{K}_{\mu 2} &= 2\cdot\mathrm{Im}\{\boldsymbol{Q}_{m_{\mathrm{v}}}^H\boldsymbol{J}_{\mu 2}\boldsymbol{Q}_{M_{\mathrm{v}}}\} \\ \boldsymbol{K}_{\zeta 1} &= 2\cdot\mathrm{Re}\{\boldsymbol{Q}_{m_{\mathrm{v}}}^H\boldsymbol{J}_{\zeta 2}\boldsymbol{Q}_{M_{\mathrm{v}}}\} \\ \boldsymbol{K}_{\zeta 2} &= 2\cdot\mathrm{Im}\{\boldsymbol{Q}_{m_{\mathrm{v}}}^H\boldsymbol{J}_{\zeta 2}\boldsymbol{Q}_{M_{\mathrm{v}}}\}. \end{aligned}$$

The two invariance equations (9) can be solved via least squares, total least squares, or structured least squares [13]. Their dimensions and the fact that $\mathcal{T}(\widehat{C}) \in \mathbb{R}^{M_{\mathrm{v}}\times 2N_{\mathrm{v}}}$ reveal that 2-D Unitary ESPRIT for near-field source localization can jointly estimate the parameters (bearings and ranges) of up to $d_{\max} = \min\{m_{\mathrm{v}},\ 2\cdot N_{\mathrm{v}}\}$ independent sources. The integer constant k_0 is chosen such that $d_{\max}$ is maximized for a given number of sensors M. In Figure 2, we have plotted these recommended values of k_0 (bottom) and the resulting values of $d_{\max}$ (top) as a function of the number of sensors M. As a comparison, recall that 1-D Unitary ESPRIT based on second order statistics can only estimate the DOAs of up to $M-1$ wavefronts if a ULA of M elements is used.

Finally, automatically paired bearing and range estimates are obtained from the eigenvalues of the "complexified" matrix $\boldsymbol{\Upsilon}_\mu + \mathrm{j}\boldsymbol{\Upsilon}_\zeta$ as discussed in [7, 8]. Let λ_i, $1 \le i \le d$, denote the complex-valued eigenvalues of $\boldsymbol{\Upsilon}_\mu + \mathrm{j}\boldsymbol{\Upsilon}_\zeta$. Then automatically paired estimates of the spatial frequency pairs $[\mu_i, \zeta_i]$ are given by $\mu_i = \arctan(\mathrm{Re}\{\lambda_i\})$ and $\zeta_i = \arctan(\mathrm{Im}\{\lambda_i\})$, $1 \le i \le d$.

4. Non-Zero Lag Cumulants

The preceding method of generating pseudo data using zero-lag cumulants is advantageous if the array size is large. Alternatively, for small array sizes, if the sources are known to have long memory, i.e., the source cumulants $c_{s_i}(\tau)$ are non-zero for all lags $\tau \in \{0, 1, \ldots, \tau_{\max}-1\}$, the cumulants $c_{p,q}(\tau, k, \ell)$ for $p = 0$, $q = 1$, can be collected for $(k_{\min}+1) \le k, \ell \le (k_{\max}-1)$, to obtain the matrix consisting of cross-cumulants

$$\mathcal{C}(\tau) = \sum_{i=1}^{d} \boldsymbol{a}(\mu_i)\boldsymbol{a}^T(\zeta_i)c_{s_i}(\tau)e^{\mathrm{j}(\mu_i-\zeta_i)}. \tag{10}$$

The arrangement in (10) is similar in form to (4) and can be used to generate a pseudo data matrix by changing the lags $\tau \in \{0, 1, \ldots, \tau_{\max}-1\}$. The URA in this case is of dimension $M_{\mathrm{v}'} = (M-2)\times(M-2)$. The pseudo data matrix generated from the cumulant matrix lags has dimensions $M_{\mathrm{v}'} \times N_{\mathrm{v}'}$ where $N_{\mathrm{v}'} = \tau_{\max}$.

The Unitary ESPRIT algorithm can be modified so that pseudo data from non-zero lag cumulants can be used to extract source parameters. In this case the maximum number of source locations that can be estimated is given by $d_{\max} = \min\{2\cdot\tau_{\max},\ (M-2)\cdot(M-3)\}$. Note that this method provides the flexibility with resolution determined by the number of non-zero cumulant lags as well as the number of sensors.

5. Simulations

To demonstrate the performance of the proposed algorithms, consider the following scenario. A ULA of $M = 6$ sensors with interelement spacing $\Delta = \lambda/4$ was used to estimate the locations of two (first order) Butterworth filtered BPSK sources with cutoff frequencies 0.3 and 0.8, respectively, located at $(\theta_1, r_1) = (20°, 5\lambda)$ and $(\theta_2, r_2) = (-5°, 1.8\lambda)$. With the SNR set to 15 dB, the number of snapshots N was varied from 128 to 8192 samples, and the results were averaged over 1000 trials. For the zero-lag version $k_0 = 0$ and the non-zero lag method used $\tau_{\max} = 3$. The resulting RMS error of the estimated DOAs (in degrees) is depicted in the top row of Figure 3, while the corresponding RMS error of the estimated ranges (in units of the wavelength λ) is depicted in the bottom row of the same figure. In addition to the performance obtained with both versions of 2-D Unitary ESPRIT (using the LS solutions of the real-valued invariance equations), we have also plotted the results achieved with the standard ESPRIT based algorithm for near-field localization proposed in [1]. The proposed algorithms, which are motivated by the ideas presented in [1], show a better performance because the centro-symmetry of the ULA is better exploited in 2-D Unitary ESPRIT as compared to the standard ESPRIT. Moreover, the range estimation accuracy of the non-zero lag version of 2-D Unitary ESPRIT outperforms the range estimation accuracy of the zero lag version since we have used a relatively small number of sensors ($M = 6$). Intuitively, the performance of zero-lag version can be expected to improve as the number of sensors is increased.

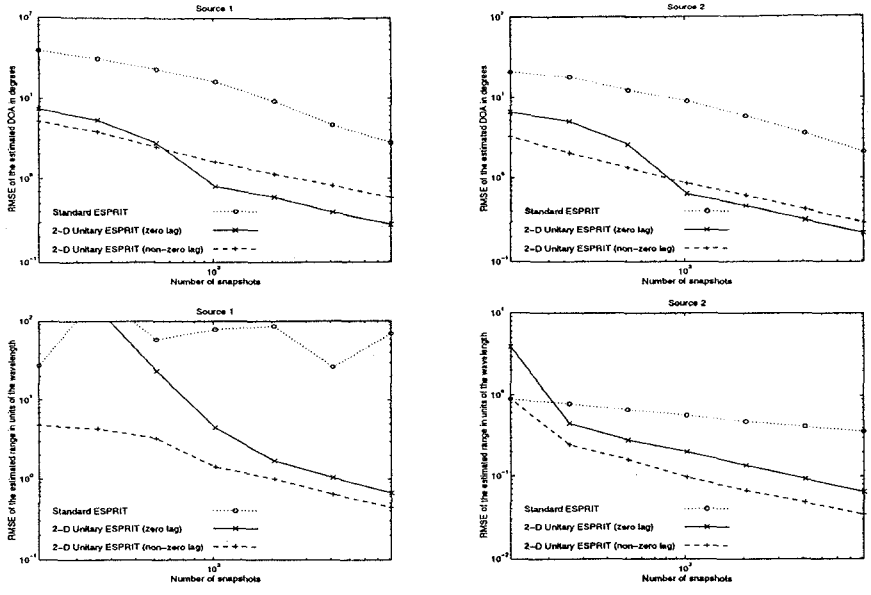

Figure 3: RMS error of the estimated DOAs (in degrees) in the top row and of the estimated ranges (in units of the wavelength λ) in the bottom row for source 1 at $(\theta_1, r_1) = (20°, 5\lambda)$ and source 2 at $(\theta_2, r_2) = (-5°, 1.8\lambda)$ as a function of the number of snapshots N ($M = 6$ sensors, $k_0 = 0$, $\Delta = \lambda/4$, 1000 trial runs, SNR = 15 dB).

Conclusions

Two new methods are proposed to passively localize near-field sources in azimuth and range. The proposed schemes exploit cumulant properties to map the data from ULA observing near-field sources to pseudo data collected from a virtual URA. The cumulant processing restores the centro-symmetric property of the ULA which is lost in the presence of near-field sources and yields the direction and range estimates of near-field sources via efficient real valued Unitary ESPRIT like algorithms. The first method based on zero-lag cumulants uses sub-arrays and is advantageous for bigger arrays and when the sources do not have long enough memory. On the other hand the second algorithm based on non-zero lag cumulants uses data from all the elements from the array and hence shows better performance for small arrays and sources with long memory.

References

[1] R. N. Challa, and S. Shamsunder, "High-order subspace based algorithms for passive localization of near-field sources," *29th Asilomar Conference*, 1995.

[2] R. Challa and S. Shamsunder, "3-D spherical localization of multiple sources using cumulants," Proc. of 8th IEEE SP workshop on Statistical Signal and Array Processing, Corfu, Greece, pp. 101-104, June 1996.

[3] D. Starer and A. Nehorai, "Passive localization of near-field sources by path following," *IEEE T-SP*, March 1994.

[4] A. L. Swindlehurst and T. Kailath,"Passive direction of arrival and range estimation for near-field sources," *IEEE Spec. Est. and Mod. Workshop*, 1988.

[5] A. Weiss and B. Friedlander,"Range and bearing estimation using polynomial rooting," *IEEE J. of Oceanic Engineering*, pp. 130-137, 1993.

[6] R. Roy and T. Kailath, "ESPRIT-Estimation of Signal Parameters by Rotational Invariance Techniques," *IEEE T-ASSP*, pp. 984-995, July 1989.

[7] M. Haardt, M. D. Zoltowski, C. P. Mathews, and J. A. Nossek, "2D Unitary ESPRIT for efficient 2D parameter estimation", in *Proc. of ICASSP*, May 1995, vol. 3, pp. 2096–2099.

[8] M. D. Zoltowski, M. Haardt, and C. P. Mathews, "Closed-form 2-D angle estimation with rectangular arrays in element space or beamspace via Unitary ESPRIT," *IEEE T-SP*, pp. 316-328, Feb. 1996.

[9] A. L. Swindlehurst and T. Kailath, "Azimuth/elevation direction finding using regular array geometries", *IEEE T-AES*, Jan. 1993.

[10] A. J. van der Veen, P. B. Ober, E. D. Deprettere, "Azimuth and elevation computation in High Resolution DOA Estimation", *IEEE T-SP*, July 1992.

[11] A. Lee, "Centrohermitian and skew-centrohermitian matrices", *Linear Algebra and its Applications*, vol. 29, pp. 205–210, 1980.

[12] M. Haardt and J. A. Nossek, "Unitary ESPRIT: How to obtain increased estimation accuracy with a reduced computational burden", *IEEE T-SP*, pp. 1232–1242, May 1995.

[13] M. Haardt and J. A. Nossek, "Structured least squares to improve the performance of ESPRIT-type high-resolution techniques", in *Proc. of ICASSP*, pp. 2805–2808, May 1996.